Revealing European-wide ecosystem strategies to drought from space

Chen, Qi; Timmermans, Joris; van Bodegom, Peter M.

DOI
10.1126/sciadv.adt9251

Publication date
2025

Document Version
Final published version

Published in
Science Advances

Citation (APA)
Chen, Q., Timmermans, J., & van Bodegom, P. M. (2025). Revealing European-wide ecosystem strategies to drought from space. *Science Advances*, *11*(31), Article eadt9251. https://doi.org/10.1126/sciadv.adt9251

ECOLOGY

Revealing European-wide ecosystem strategies to drought from space

Qi Chen[1]*, Joris Timmermans[1,2], Peter M. van Bodegom[1]

Ecosystems are threatened by increasing droughts under climate change. A multitude of plant physiological regulation processes determine the overall drought resistance of ecosystems. So far, these physiological strategies to resist drought are poorly understood at large scales across different ecosystem types because the detection of these physiological regulation processes is mostly limited to in situ measurements on individual plants. In this study, by using high-resolution remote sensing data, we evaluated drought strategies of different ecosystem types throughout Europe by evaluating three key physiological regulation aspects (evapotranspiration, water content, and carbon regulation) based on their associated vegetation attributes. We found that different ecosystem types show divergent responses in these physiological attributes, suggesting different optimization strategies with respect to water saving versus spending, water content stabilizing versus fluctuating, and leaf conserving versus shedding strategies facing drought. These drought strategies from remote sensing provide timely ecosystem response information, facilitating earth system model predictions and aiding the protection against future droughts at large scales.

INTRODUCTION

Ecosystems are likely to be increasingly threatened by more frequent and severe droughts under climate change (*1*–*3*). These droughts can affect multiple physiological processes in vegetation, thus impairing their ability to adapt to severe drought and even leading to mortality, which will ultimately affect the structure and functioning of entire ecosystems (*4*–*6*). The regulation of various physiological processes in vegetation forms the basis of their drought resistance strategies, and the identification of these strategies constitutes a priority in global research efforts (*7*–*9*). However, much of the current understanding on plant strategies in response to drought is based on responses by individual plants at individual sites (*10*–*13*). It is still unclear how these strategies translate to the whole ecosystem level and how they vary across different ecosystems. Moreover, current predictions of future vegetation response and mortality mostly rely on sparse ground vegetation data, resulting in substantial uncertainty in the predictions (*14*). To accurately predict the subsequent ecological impacts of drought events and to effectively address the threats induced by global climate change, it is crucial to understand drought strategies in detail at the ecosystem level across large scales (*15*).

For individual plant species, strategies during drought can generally be classified through three key interlinked physiological regulation aspects: stomatal regulation, water content regulation, and carbon regulation. These regulations are closely linked to the two main mechanisms of plant mortality (i.e., hydraulic failure and carbon starvation) (*16*, *17*). Consequently, much research has been done to explore drought strategies by identifying individual regulation aspects for specific species (*11*, *18*–*20*). Regulation of plant water content has so far received most attention in characterizing plant drought strategies. Such hydraulic strategies are commonly classified along an axis from water conservation (drought avoidance or isohydric species) to water spenders (drought tolerance or anisohydric species) (*11*). Isohydric species are those that maintain their leaf water potential (Ψ_{leaf}) and avoid dehydration during drought, whereas anisohydric species decrease their Ψ_{leaf} with decreasing soil water availability and suffer greater dehydration (*18*, *21*). Regulation of stomata (i.e., stomatal control) was thought to be closely related to the hydraulic strategy (*22*) because the dynamic behavior of stomata in regulating water loss dictates the rate of plant dehydration as soil water availability declines (*23*). However, the exact relationship between stomatal regulation and water content regulation for isohydric versus anisohydric species remains uncertain and is still facing controversies (*23*–*25*). Regulation of carbon is key to the second mechanism to respond to drought. Plant species can optimize their overall response to drought through a physiological trade-off between minimizing water loss and maximizing carbon gain at the leaf level (*26*). For instance, plants may shed leaves during drought (i.e., regulate their carbon balance) to prevent hydraulic failure (*27*–*29*). Different ecosystem types may regulate their physiological responses differently, ultimately determining their resistance to drought and possible mortality patterns. However, till now, evaluation of all these three regulation aspects simultaneously in different ecosystem types is still lacking.

While previous studies have established an understanding of drought strategies and their links to the three aspects of regulation at the individual plant level, understanding at the ecosystem level across different ecosystem types is still limited, due to the challenges in upscaling strategies from individual tissues to the whole-plant and community level (*24*). In light of the importance of vegetation drought strategies to the global carbon balance and the expected changes in drought dynamics with climate change, it is critical to provide accurate and timely information on strategies at these large scales to improve drought response predictions (*30*–*32*). This is particularly relevant because ecosystem strategies can vary with species composition and local environment conditions (*33*–*35*). Thus, consecutive monitoring is needed to comprehensively assess drought-related responses and their variations in space and time. Remote sensing with its large-scale monitoring and quick revisit times provides the possibility to solve these challenges, and efforts have been made to evaluate vegetation responses to drought using remote

[1]Institute of Environmental Sciences (CML), Leiden University, Box 9518, 2300 RA Leiden, Netherlands. [2]Faculty of Civil Engineering and Geosciences, Technical University Delft, 2628 CN Delft, Netherlands.
*Corresponding author. Email: q.chen@cml.leidenuniv.nl

sensing (*36*). For instance, attempts have been made to evaluate hydraulic responses of vegetation using vegetation optical depth (VOD) data (*37*, *38*). Large-scale estimates of evapotranspiration (ET) and carbon-related responses have also been evaluated with remote sensing data (*39*–*44*). While various studies have focused on one or two types of regulation, recent efforts have advanced toward monitoring multiple aspects of plant regulation simultaneously using remote sensing (*45*). However, most large-scale assessments of multiple vegetation responses to drought have relied on data at 25-km spatial resolution, and less attention has been paid to the evaluation of tradeoffs between multiple key physiological regulation aspects at the ecosystem level. Thus, analyses to distinguish drought strategies at the ecosystem level are strongly needed through the use of high-resolution data.

Here, we evaluate multiple physiological responses to drought at ecosystem level and assess to which extent these ecosystem strategies are affected by increasing drought through high-resolution remote sensing data. To this end, we first analyzed the meteorological drought conditions during the unprecedented 2018 drought in Europe. To explore drought strategies, three key aspects of physiological regulation during drought were expressed as canopy-level responses in three attributes: loss in ET, loss in water content, and loss in leaf area. These attributes were derived by remote sensing proxies to enable full spatial coverage across Europe (at 1-km resolution) and to characterize their temporal dynamics. The decrease in actual ET was used to evaluate the regulation of ET. Likewise, the decrease of the normalized difference infrared index (NDII) was used to indicate the regulation of canopy water content. The decrease in leaf area index (LAI) was used as a proxy for leaf area loss, indicating the regulation of carbon dynamics (Fig. 1). Based on these attributes, we ask: (i) How do different ecosystem types regulate the three physiological attributes to cope with drought? (ii) Does the onset of regulation in the three attributes within an ecosystem type shift with increasing drought severity? and (iii) Does the magnitude of regulation in the attributes of a given ecosystem type change with increasing drought severity?

RESULTS

Divergent drought strategies across ecosystem types

Three aspects of regulation in terrestrial ecosystems during drought were evaluated (Fig. 2). The first regulation (i.e., loss in ET) represents drought impacts on water release from ecosystems, as indicated by accumulated ET decrease (and is partly related to stomatal regulation). Ecosystem types exhibit divergent ET responses to drought, from those with an early and high ET decrease to those with delayed and limited ET reduction or those with a minor decrease in ET over time (Fig. 2); that is, they vary from a more conservative water loss strategy (water saver) to a looser water loss strategy (water spender).

The second regulation (i.e., loss in NDII) represents the dynamics of canopy water content during drought, referring to the ability to maintain a high or low water content level, which is related to the

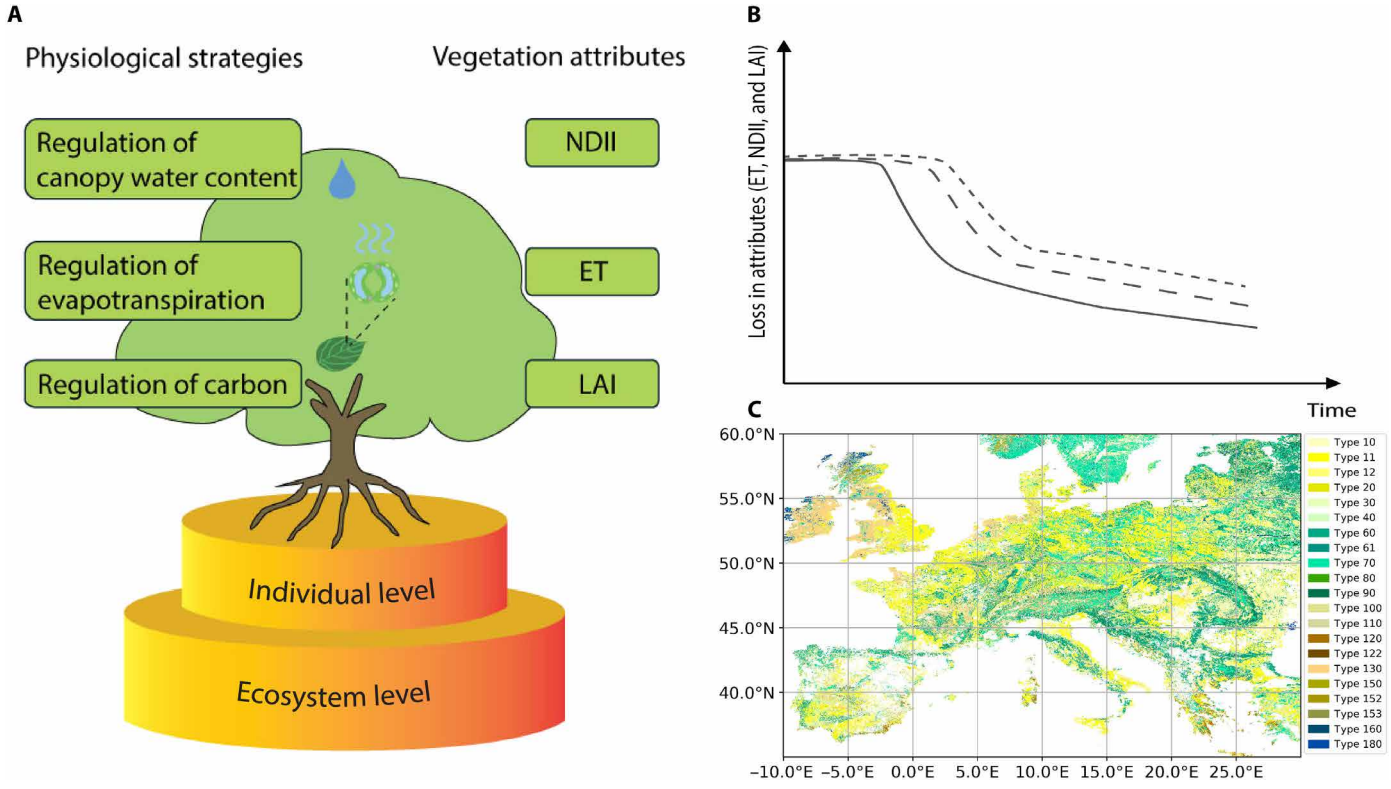

Fig. 1. Overview of the study. (**A**) Physiological strategies of plants upon drought and the corresponding vegetation attributes (derived by remote sensing proxies) that can be used to reflect their regulation. ET, evapotranspiration; NDII, normalized difference infrared index; LAI, leaf area index. (**B**) Hypothesis on drought strategies monitored by remote sensing. Vegetation attributes will show loss at different time points and to different magnitudes due to the specific regulatory sequences of plants facing drought. (**C**) European ecosystem distribution map. The names of ecosystems can be found in table S1 by type number.

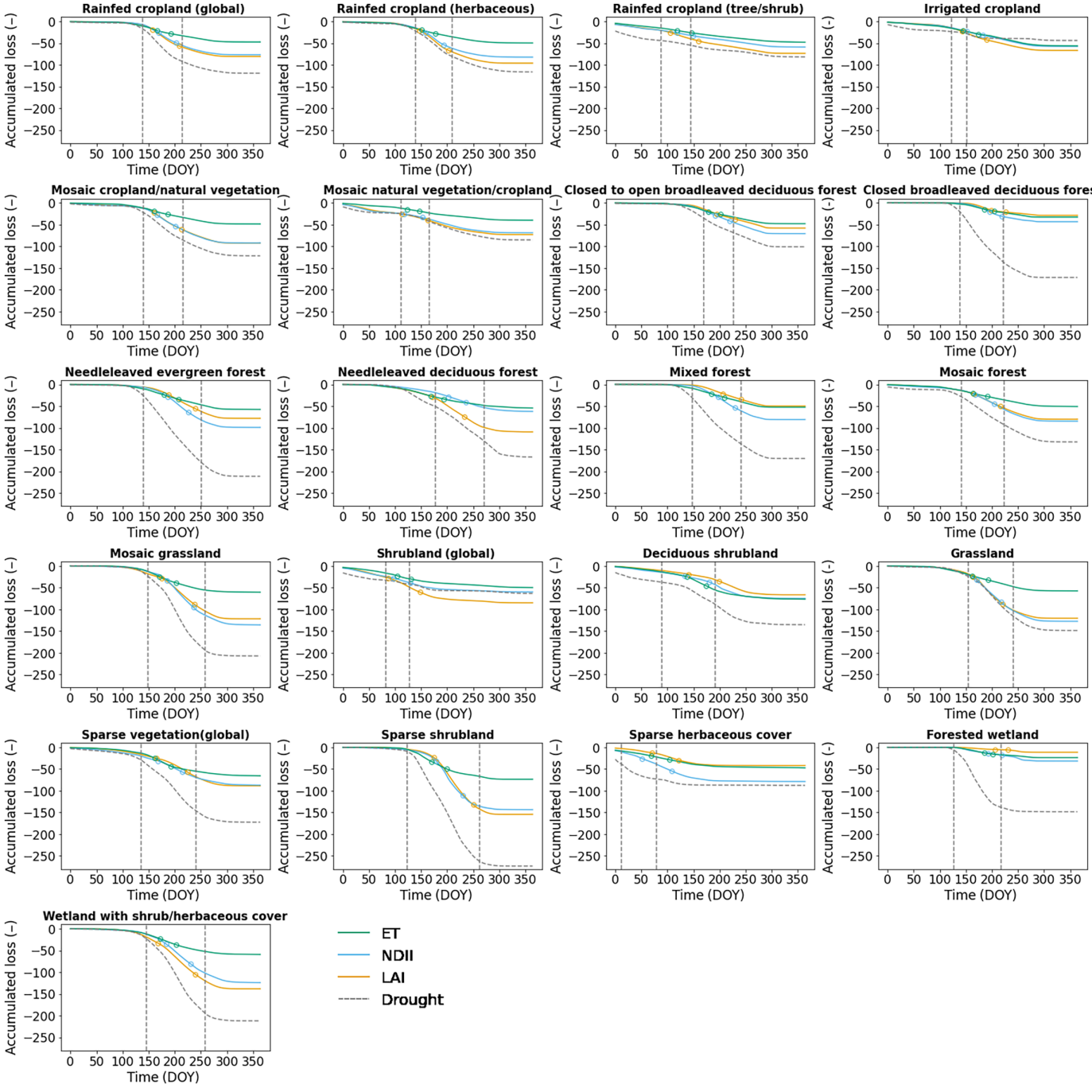

Fig. 2. Three aspects of regulation in different ecosystem types across Europe in response to drought. The severity of drought (dashed line) and the response in regulation of ET (green line), NDII (blue line), and LAI (orange line) with time (expressed as DOY, day of year) in 2018 (see Materials and Methods for calculation details). Loss in a vegetation attribute indicates the decrease in that attribute in 2018 compared to previous years. The accumulated losses in these attributes were obtained by summing the decreases in ET, NDII, and LAI over time. Negative values at a given time point indicate the total accumulated loss in the vegetation attribute till that moment. Here, the circles represent the mean onset and end date of vegetation loss in each ecosystem type. The two vertical dashed lines represent the mean onset and end date of drought in each ecosystem type. The onset and end date of vegetation loss and drought were defined as the start date and end date of the longest vegetation loss and drought event, respectively.

plant water potential (*46*–*49*). NDII responses vary from ecosystem types with a late and low water content decrease to types with an early and high water content decrease, corresponding to either a stabilizing or a fluctuating strategy of water content regulation (these strategies do not directly reflect the isohydric-anisohydric degree but partly indicate the variation in plant water potential) (Fig. 2).

The third regulation based on the key attribute LAI reflects the carbon loss of ecosystems upon drought. Leaf shedding as "hydraulic fuses" is a key mechanism for plants to cope with drought (*27*, *50*). Also this regulation varies across ecosystem types from those with low LAI decreases to ones with high LAI decreases (Fig. 2), indicating a biomass maximization strategy trying to keep normal growth during drought versus those that shed leaves as a risk limitation strategy.

Somewhat unexpectedly, the three regulation aspects mostly covaried with increasing drought, indicating limited capabilities of canopies to adjust only one physiological process at a time (Fig. 2). However, this covariant relationship varies across different ecosystems, with some ecosystem types being able to more independently change regulation in different attributes than others (most types show significant differences in accumulated loss in ET, NDII, and LAI at the middle and the end of drought with a paired *t* test) (table S2). This indicates that the extent to which a trade-off between ET, control of water content, and carbon loss was expressed varied among ecosystem types. For instance, croplands showed a large decrease in LAI and NDII, which dropped faster than ET, except for rainfed croplands with trees and shrubs. This indicates that, although crops decrease their ET, they cannot maintain their biomass and water content during drought. In contrast, forests showed the capability to maintain one attribute (LAI or NDII) longer than crops with an early ET decrease. Specifically, mixed forests showed a late and low LAI decrease, indicating their capability of biomass maximization during drought. They showed a propensity for a more conservative stomatal regulation strategy (early ET anomaly onset and high ET decrease) and a more variable water regulation strategy (high water content decrease). On the other hand, needleleaved deciduous forests showed a late and low decrease in canopy water content, which seems to come at the cost of more leaf shedding.

Ecosystem types with low vegetation cover showed distinct responses to drought (Fig. 2). Ecosystems with sparse herbaceous cover first decreased canopy water content, then ET, and lastly reduced their leaf cover. In contrast, sparse shrublands first decreased ET while keeping their canopy leaves and water content for a longer period. It seems that the growth form dominating sparse vegetation is important in determining the drought strategy. Forested wetlands showed a water spender strategy. They could maintain their biomass with a little decrease in ET and canopy water content, while wetlands with a shrub or herbaceous cover showed a reaction similar to that of terrestrial grasslands. Grasslands also showed similar strategies to croplands.

Shift in the temporal sequence of regulation with enhanced drought severity

We analyzed the changes in the onset of decreases in three vegetation attributes (indicated by ET, NDII, and LAI) along with increasing drought severity to explore whether ecosystems adapt their strategy to deteriorating drought conditions. We observed that most ecosystem types showed a consistent sequence in the reaction of the three canopy-level attributes, which barely showed any change with drought severity.

Despite the consistent reaction of most ecosystem types, some ecosystem types show an earlier loss in carbon (i.e., earliest onset in LAI decrease) to increased drought stress and lose control of their ideal strategies (Fig. 3). Crops and forests all first tried to decrease their ET under mild drought conditions, while with increasing drought severity, crops could not afford to maintain their water demand and were forced to decrease their LAI quickly and strongly. Most forests could maintain their regular canopy response sequence at severe drought. For example, needleleaved evergreen forests and mixed forests decreased ET earlier than LAI and NDII across all drought severity conditions. Mixed forests showed a late reaction of LAI across all drought severity conditions, which indicated their strategy to maintain their biomass, which is barely affected by drought conditions. Needleleaved deciduous forests showed hardly any diminution in the onset of canopy water content response across all drought severities, matching with their early decrease in LAI. However, compared to these stable forests, closed to open broadleaved deciduous forests showed an early shift in the onset of responses in their three canopy attributes. Their LAI was affected earlier than the other two attributes with increasing drought severity, representing a major change in the strategy for this ecosystem type and a failure to maintain their strategy. This phenomenon also emerged in grasslands. Benefiting from a wet growing environment, forested wetlands kept their water spender strategy even under severe drought.

Forested wetlands and needleleaved deciduous forests showed largely distinct onsets in the responses of the three vegetation attributes (Fig. 3 and fig. S1). This indicates that these ecosystem types have the ability to independently regulate each of the three canopy-level attributes. This may allow them to fine-tune their response to drought, in contrast to other ecosystem types where responses in the three attributes mostly covary.

Changes in the magnitude of regulation with enhanced drought severity

In addition to the order in which declines in one vegetation attribute occur (i.e., the changes in the onset), the magnitude of regulation in vegetation attributes constitutes another key aspect of ecosystem responses to drought. To evaluate whether this magnitude of decline will be stable under severe drought, we analyzed the slopes (i.e., sensitivity) of the magnitudes in the three canopy attributes to changing drought conditions (Fig. 4 and fig. S3). We found that all three attributes showed a similar overall sensitivity to drought for a given ecosystem type. Only subtle differences occurred in some types (e.g., crops) between ET and the other two attributes. This analysis reinforces the conclusion of the previous section that most ecosystems have stable plant strategies across drought severity ranges except for the vulnerable ones.

In general, crops were the most vulnerable types in the responses of all three canopy attributes and showed the highest sensitivity (i.e., the steepest slopes) to drought compared to other ecosystem types (Fig. 4). This high sensitivity to deteriorating drought conditions reflects their difficulty to maintain a stable strategy. They failed to keep their LAI under severe drought, which was consistent with their early shift in the onset of the responses in the three attributes with increasing drought severity. Forests showed a lower sensitivity (i.e., flatter slopes) than most other types and showed a more stable strategy minimizing the impact on LAI across all drought severity levels (i.e., the LAI line is the lowest of all three lines). In particular, for mixed forests, LAI responded less than the other two canopy attributes when compared with other forests. Grasslands showed a higher sensitivity than forests but lower than croplands in these three

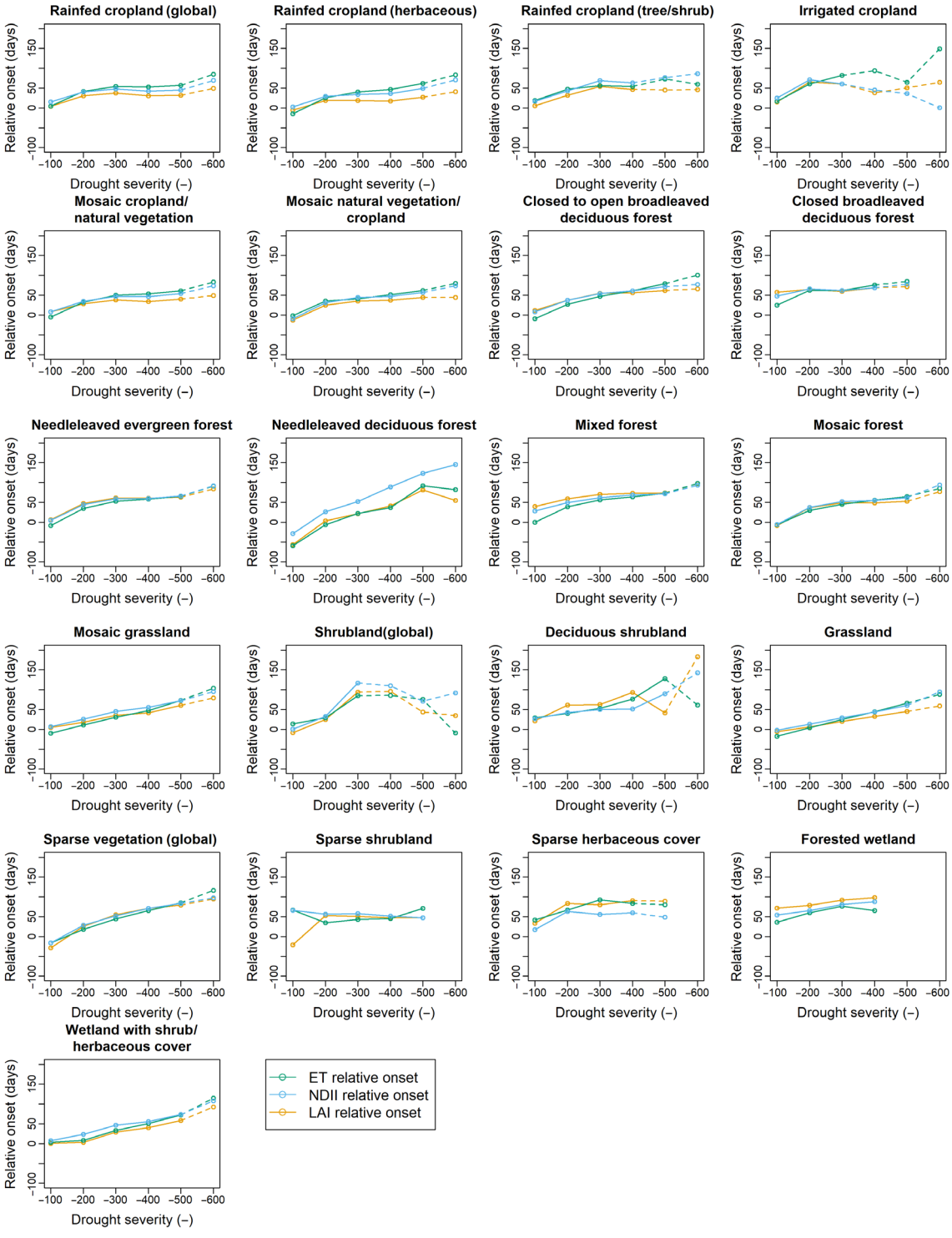

Fig. 3. Changes in the relative onset of decreases in ET, NDII, and LAI with drought severity. The relative onsets represent the time difference between the onset of vegetation decrease and the onset of drought. Vegetation decrease was determined based on anomaly values of ET, NDII, and LAI in 2018 compared to values from previous years. Drought was identified as periods with SPEI values lower than −0.5. The onset of vegetation decrease and drought was defined as the start date of the longest vegetation anomaly and drought event, respectively. For more details about the definition of these onsets, see Materials and Methods. These relative onsets were averaged for a given drought severity per ecosystem type. The dashed lines represent patterns for extreme drought severity (less than the 1st percentile). The spatial pattern of these onsets in Europe can be seen in fig. S4.

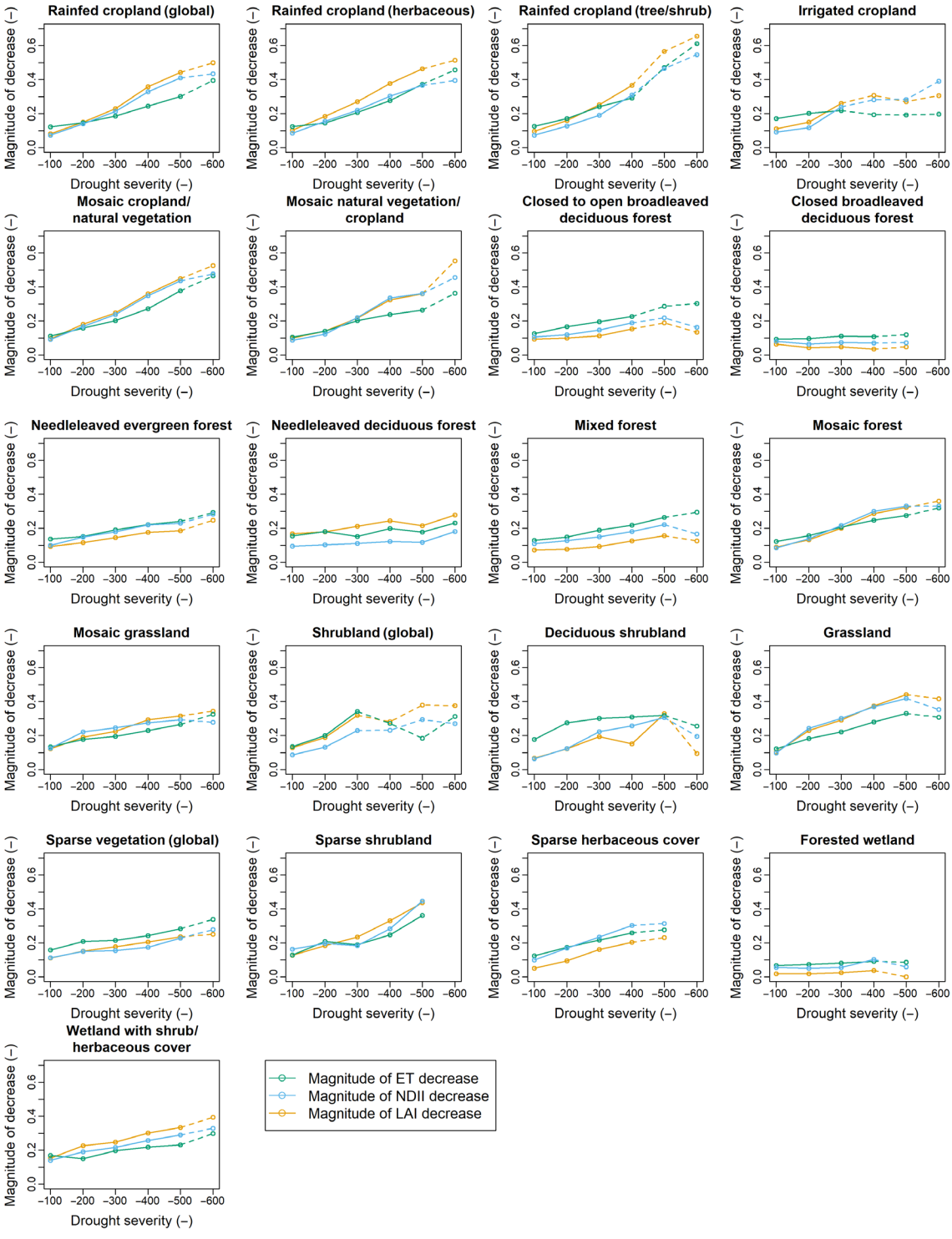

Fig. 4. Changes in the magnitude of decreases in ET, NDII, and LAI with increasing drought severity. The magnitude of vegetation decrease was calculated on the basis of the severity of ET, NDII, and LAI changes (defined as the sum of standardized anomaly values lower than −1) in 2018 compared to values from previous years. The average magnitude of the decrease in ET, NDII, and LAI was calculated for each drought severity level. All magnitude values were first scaled to 0-1 by min-max normalization. The slopes of these lines represent the sensitivity to drought severity for each ecosystem type. The dashed lines represent data beyond the value at the 1st percentile of drought severity. The spatial patterns of these vegetation responses in Europe can be seen in fig. S4.

canopy attributes. They also failed to minimize the impact on LAI under severe droughts. We found highly consistent patterns for the magnitude (Fig. 4) and the onset of vegetation decrease (Fig. 3), with vegetation attributes that declined early showing much stronger decreases than other attributes.

To test whether vegetation responses were different between arid and humid regions, we analyzed the onset and the magnitude of decreases in the three canopy attributes across drought severity for arid and humid regions separately (figs. S5 and S6). We found that, in general, ecosystem types in humid regions showed a higher sensitivity to drought compared with those in arid regions, especially for herbaceous vegetation. Under the same drought severity, most ecosystem types in humid regions showed earlier and more severe responses to drought in the three canopy attributes compared with those in arid regions. However, no differentiation in responses between humid and arid regions was evident for forests.

DISCUSSION

Differential ability of ecosystems to regulate carbon and water upon drought

We have extended previous research by evaluating drought strategies of vegetation at the ecosystem level, by integrating the regulation of water (i.e., ET and water content) and carbon (leaf area) under drought using high-resolution remote sensing data. Specifically, we simultaneously assessed responses in three key physiological attributes: regulation of ET (reflecting water loss adaptation), regulation of canopy water content (reflecting water retention capacity), and regulation of leaf area (reflecting leaf shedding and photosynthesis behavior). This combined evaluation at ecosystem level facilitates a comprehensive assessment of vegetation responses to drought. Our evaluation shows that the regulation of the three physiological attributes tends to covary strongly, suggesting that it is difficult to have independent strategies for individual attributes. However, this coordinated regulation in the three attributes differs among ecosystem types in terms of the sequence of response and the magnitude to which regulation is possible. These insights provide a valuable way to understand vegetation strategies in diverse ecosystems during drought.

Most ecosystems first reduce their ET to avoid carbon loss and to maintain their regular canopy functioning. The preservation of canopy leaf area within these ecosystems probably reflects the importance of carbon regulation for vegetation functioning. However, most ecosystems may fail to avoid carbon loss with increasing drought. The moment at which the canopy leaf area starts to drop differs among ecosystems. The differences among ecosystem types in their capacity to maintain carbon regulation reflect their strategies to deal with drought.

Among forests, broadleaved deciduous forests showed the earliest collapse in water and carbon regulation (Fig. 3). Drought strategies commonly differ between broadleaved and needle-leaved species. Broadleaved deciduous forests shed their leaves early during drought to reduce transpiratory water loss (*51*), thereby protecting the integrity of the water transport system in their stem (*28*, *52*). This integrity is crucial because damage to the hydraulic system may result in embolism and, ultimately, lead to tree mortality (*16*, *53*, *54*). Broadleaved deciduous forests usually have high photosynthetic rates, and their foliage can be restored in the next growing season (*55*, *56*). Needleleaved evergreen forests, in contrast, cannot afford such extensive carbon loss. They have greater leaf construction costs (*57*) and conservative ET strategies (*58*). It is not until severe drought, causing stomatal closure, that they have to drop leaves as a last chance for hydraulic safety (*50*).

Mixed forests showed the latest collapse in their regulation compared to other terrestrial forests (Fig. 3). In particular, mixed forests try to maintain their canopy leaf area by reducing ET and water content. Mixed forests contain diverse drought strategies with their diverse species composition (*59*, *60*), which can make the forests benefit from compensating mechanisms through resource partitioning and facilitation (*59*, *61*, *62*). For example, broadleaved forests usually have high stomatal conductance allowing for continued carbon gain and water use during drought, which cools the entire system and reduces the evaporative demand of other trees (*63*). Similarly, the interspecific variation in rooting strategies of different species can improve local soil water availability or the microclimate for trees through active hydraulic redistribution and nocturnal water transport (*64*–*66*). In combination, this explains why mixed forests usually exhibit more stable canopy attributes during drought.

We particularly observed clear differences between forested and non-forested ecosystem types. Specifically, croplands and grasslands could barely keep their LAI and NDII by attenuating ET during drought and were forced to lose carbon early and strongly even under mild drought (Figs. 3 and 4). In contrast, most forests can keep their LAI longer and better during drought. Forested and non-forested ecosystems differ in their resource allocation. The first difference relates to their canopy height. There is evidence that vegetation canopy height has a strong causal effect on water use strategies, leading to a higher water use efficiency in forests than in grasslands (*67*). Canopy height influences surface roughness and aerodynamic resistance and hence controls the interaction between the vegetation surface and atmosphere, affecting the water use efficiency (*67*, *68*). Canopy height also affects water use efficiency due to an increasing hydraulic limitation on stomatal conductance in higher trees (*69*). In addition, higher water use efficiency of trees than grasses is also related to their high construction costs because they must invest more in building structures and, hence, a higher carbon cost of water use (*70*). Another difference relates to their rooting depth. The deep roots of trees allow them to absorb water from the deep soil (*71*), and the delayed decline in deep soil moisture can help them to keep their strategy longer. Grasslands can only absorb water from top-middle layers and are more sensitive to water deficits (*72*).

Similar differences in canopy height and rooting depth between trees and grasses explain the variation in the stability of vegetation strategies in wetlands. The relatively wet conditions of wetlands did not lead to different regulation of wetland grasses compared to that of terrestrial grasslands. However, the wet conditions seem to provide trees a higher stability. Wetland trees showed the most stable strategy with increasing (meteorological) drought severity compared with other ecosystems (even more stable than trees in mixed forests), and they showed a very late and minor LAI decrease during drought (distinct responses in ET, NDII, and LAI). Possibly, the shallow water table in wetlands still allowed the tap roots of trees to reach it even during dry conditions (*73*). Moreover, the enhanced allocation to roots among some wetland trees can provide them with the ability to remain in contact with a declining water table (*74*, *75*). In contrast to these trees, wetland grasses do not have the extensive roots of most woody plants and are, therefore, more susceptible to water shortages (*76*). Increasing occurrences of droughts, therefore, constitute a major threat of woody encroachment to global wetland grasslands (*77*, *78*).

Forested and non-forested ecosystem types also differed in their responses to drought between arid and humid regions. Non-forested ecosystem types are more sensitive to drought in humid regions compared to those in arid regions. This may be linked to the long-term adaptation of herbaceous vegetation inhabiting arid regions, such as more negative wilting leaf water potential (*79*), laterally extensive root systems (*80*), or deep root systems (*80*). Water use in forested ecosystem types tends to be relatively stable with their deep root systems (*81*), showing limited regional variation in their responses to drought. Despite the different sensitivity of non-forested ecosystem types in arid and humid regions, we found that drought severity had a stronger impact on vegetation anomalies than long-term aridity (table S3).

Coupling of water and carbon regulation

Despite the differences in the onset and magnitude to which ecosystem types were able to maintain their water and carbon regulation (represented by ET, NDII, and LAI), within one ecosystem type, these three attributes exhibited a concomitant pattern in response to drought (Fig. 2). As the severity of drought increases, they tended to exhibit a similar sensitivity across water and carbon regulation (slopes in Figs. 3 and 4). This indicates that the carbon and water cycle are tightly coupled at the vegetation level in the face of drought.

Needleleaved deciduous forests exhibited a clear difference in their water and carbon regulation compared to other ecosystem types (where water and carbon regulation were coupled). Needleleaved deciduous forests showed a much later decrease in onset and a lower reduction in canopy water content than in canopy leaf area (Fig. 4 and fig. S2). Facing drought, they first reduced their leaf area. They even maintained their canopy water content after dropping their leaves, which indicates they increased the water content per leaf.

The dominant species in coniferous deciduous forests in our study area is the European larch (*82*, *83*). According to on-site measurements and experimental research, drought has a low impact on the water content and water usage in *Larix decidua* (*84*–*86*), while it has a substantial inhibitory effect on its growth (*87*–*89*). One reason why they can maintain a high water content during drought is their ability to use water in deep soil because of their deep rooting system (*90*). Another reason is related to their unique drought regulation mechanism: They can decrease their water potential through osmotic adjustment (i.e., accumulate solutes within their cells), which also increases the water uptake capacity of the plants since it facilitates a lower water potential up to the fine roots (*84*). Consequently, they can keep their water content during drought. Therefore, this high water content does not mean a high water potential or a more isohydric behavior. In contrast, they have a lower water potential and a more anisohydric behavior in drought because of their unique osmotic regulation mechanism (*85*, *91*, *92*).

Implications for future drought management: Opportunities and limitations

The combined assessment of the regulation in three key canopy-level physiological attributes allowed for integrally assessing the strategy of vegetation across ecosystem types. Drought affects both carbon and water regulation in ecosystems and, to a major extent, simultaneously with a primacy of carbon regulation where possible. The comprehensive strategy evaluation of ecosystems, provided in this study, can further deepen our understanding of the key carbon and water responses by ecosystems to drought.

Where different strategies prevail, this will affect carbon and water cycling. Till now, these differential effects caused by different plant strategies are not represented in most dynamic vegetation models (DVMs) (*8*). Plant strategies have been suggested to be incorporated into global vegetation models to describe the impact of drought on carbon cycling more accurately (*8*, *93*) but were, so far, considered a huge challenge (*8*, *94*). The traditional measurements of plant strategies only provide information for certain conditions and locations, which makes it difficult to inform large-scale simulations. In addition, the traditional measurements are limited in assessing the temporal dynamics of strategies. The dynamic responses of ecosystems to climate and environmental variability could thus be poorly assessed. Such dynamic assessments are important, given that the frequency and severity of droughts caused by global warming are projected to increase in the future (*2*, *95*), leading to possible increases in the mortality of forest trees (*96*, *97*). The death of these trees will reshape the ecosystem's original responses and strategies (*33*, *98*), which will have a substantial impact on ecosystem functions and on the overall global carbon and water balances (*99*). In view of these changes, it is crucial to achieve a real-time integral monitoring of ecosystem strategies.

Here, we used high-resolution remote sensing to monitor vegetation strategies at ecosystem level to capture the real-time expression and changes in vegetation strategies associated with drought. It provides large-scale, integrated information on drought response strategies and serves as structural input or constraints for DVMs and earth system models. These will provide critical support for drought impact predictions on carbon and water regulation of ecosystems at a global scale, contributing to a better understanding of future climate change impacts on carbon and water cycling. Moreover, the observed real-time strategies may timely reflect the health status (i.e., water shortage and carbon loss status) of ecosystems and, hence, will provide a theoretical basis for formulating effective drought policies and water allocation strategies in the face of drought in the future.

Using remote sensing for large-scale vegetation strategies monitoring still faces uncertainties and challenges. Remote sensing variables generally capture ecosystem-level responses, but it remains difficult to directly evaluate vegetation responses at the level of specific physiological traits, such as stomatal behavior, osmotic adjustment, or root distribution. ET was used as a proxy for canopy water use loss in this study. While plant stomatal conductance influences transpiration (*100*), ET can also be affected by other plant physiological changes (e.g., leaf area) and nonphysiological factors, including changes in bare soil fraction and fluctuations in energy supply (net radiation, air temperature, wind speed, and humidity) (*101*–*103*). Thus, ET regulation only partially reflects stomatal control behavior. NDII, calculated from near-infrared (NIR) and shortwave infrared (SWIR) reflectance, has been shown to be sensitive to vegetation water content, due to strong water absorption features in the SWIR bands (*104*, *105*). Many studies have shown that NDII correlates with leaf and canopy water content and has been used to indicate vegetation water conditions under water stress (*105*–*108*). A decrease in water content normally leads to a more negative water potential (*46*–*48*). However, the variation of water content can sometimes be decoupled from water potential due to special regulatory mechanisms in plants during drought, such as osmotic adjustment (*84*). Moreover, NDII alone lacks information about soil water conditions. Therefore, NDII does not directly reflect the isohydric degree of plants, while it indicates their water content regulation behavior.

Based on the comparison between NDII and VOD (daytime) reduction during drought, we found that NDII is generally able to capture changes in vegetation water content in ecosystems (fig. S8B). However, the ability of NDII to indicate water content can decrease in areas with low vegetation fraction, due to the increased influence of soil background reflectance and covariation with the biophysics of plants (e.g., leaf area and leaf structure) (*109*, *110*). These effects of soil background reflectance, especially the influence of soil moisture variation, can also increase the uncertainties in the other two variables (ET and LAI) in areas with sparse vegetation (*111*, *112*). Despite these uncertainties, we found that, for most ecosystem types, ET and LAI data from remote sensing showed wide agreement with eddy covariance ET and gross primary productivity (GPP) measurements (fig. S7). Meteorological drought was the focus of this study, assessed on the basis of deficits between precipitation and potential evapotranspiration (PET). Vegetation responses were used as an indicator of ecological drought, reflecting the impact of actual water deficits on the ecosystem. Meteorological drought can become decoupled from actual soil water deficits in regions affected by additional water inputs, soil properties, or microclimate variability (*113*). The weak responses observed in some ecosystem types may partly reflect relatively low soil water deficits during drought events, such as shown by the relatively low vegetation responses in forested wetlands.

In summary, our analysis shows how different ecosystem types exhibit different responses to drought in the regulation of ET, canopy water content, and leaf area. Specifically, ecosystem types show different preferences to keep one attribute (water loss, water content, or biomass) more stable and, in this way, show their overall strategy as water saver versus water spender, stable water content versus fluctuating water content, or biomass keeper versus leaf shedder. Even so, while these differences in preferences are present, in general, the regulation in three canopy-level attributes strongly covary, suggesting a close coupling of water and carbon regulation. Moreover, ecosystems barely change their drought strategy with deteriorating drought conditions. However, vulnerable ecosystem types may lose control at a certain point. Specifically, crops are the most sensitive types in coping with drought, and they fail to keep their biomass and water content stable even during mild drought. On the other hand, most forests can keep their strategy stable along the entire drought severity range with minimum decrease of individual vegetation attributes. The comprehensive monitoring developed here can be used to detect drought strategies at ecosystem level and can be applied to future studies to reveal drought impacts. This also provides timely information on ecosystem strategies to drought, allowing for improved predictions in DVMs and earth system models on continental and global scales.

MATERIALS AND METHODS

Data processing

Drought events were characterized by the daily standardized precipitation evapotranspiration index (SPEI) for Europe in 2018. We chose SPEI as meteorological drought index instead of soil drought which is related more directly to vegetation responses. Soil drought demands soil moisture estimates at high resolution with long time series, which were either unavailable or insufficient for the study. SPEI was calculated on the basis of an upscaled precipitation dataset [Monitoring Agricultural Resources (MARS) precipitation data from the Joint Research Centre (JRC) upscaled by Meteosat Second Generation-Cloud Physical Properties (MSG-CPP) precipitation data from the Royal Netherlands Meteorological Institute] (*114*) and Moderate Resolution Imaging Spectroradiometer (MODIS) MOD16A2 PET data (*115*) from 2004 to 2018. For more information regarding the SPEI product, refer to (*116*, *117*).

To quantify the vegetation responses to droughts, we calculated their anomalies on the basis of data from 2004 to 2018. The standardized anomaly in ET (SAET) was calculated with 10-day 1-km resolution actual ET data from the Operational Simplified Surface Energy Balance (SSEBop) ETa product (*103*) (https://earlywarning.usgs.gov/fews/product/461/). To reduce the anomaly noise of the ETa data, a running filtering method was used to improve the smoothness of the trend. In this method, a Savitzky-Golay filter (*118*) was used to get the threshold of elimination. ET data were validated by comparison with 10-day ET values calculated from latent heat flux and air temperature measurements from eddy covariance towers. Among the 73 eddy covariance flux sites provided by the Integrated Carbon Observation System (ICOS)–Warm Winter 2020 dataset (*119*), the 13 sites that provided continuous observations from 2004 to 2018 within our study area were selected for validation. The original latent heat flux and air temperature data were quality-controlled and gap-filled using the Marginal Distribution Sampling (MDS) technique following the standardized ONEFlux processing pipeline (*120*, *121*). For comparison, the 1-km resolution pixels in the SSEBop ET dataset corresponding to the locations of the in situ eddy covariance sites were selected on the basis of the general footprint of flux towers. SSEBop ET and ICOS ET exhibited a strong correlation [correlation coefficient (r) = 0.71] across all ecosystem types during 2004–2018 (fig. S7A).

The standardized anomaly in NDII (SANDII) was calculated with NDII data produced on the Google Earth Engine (GEE) platform (*122*). NDII was usually used as an indicator of the changes in canopy water content (*105*) derived on GEE (*108*). We calculated the NDII index on GEE on the basis of the normalized difference value of band 2 (NIR, 841–876 nm) and band 6 (SWIR, 1628–1652 nm) of Modis MOD09A1 (*123*). The equation is as follows

$$\mathrm{NDII} = \frac{\mathrm{NIR} - \mathrm{SWIR}}{\mathrm{NIR} + \mathrm{SWIR}} \quad (1)$$

Before this calculation, a mask was first used to MOD09A1 surface reflectance data to remove cloud, snow, and water effects. After the calculation, values less than the 5th percentile and larger than the 95th percentile of the entire 15-year NDII data series in each pixel were removed to reduce noise. The NDII dataset from GEE was produced at 8-day and 1-km resolution.

The standardized anomaly in LAI (SALAI) was calculated with the GEOV2 LAI data (from the Copernicus Global Land Service) (*124*) (https://land.copernicus.eu/en/products/vegetation/leaf-area-index-v2-0-1km). The LAI products are available each 10 days at 1 km resolution. Similar to the validation of the ET data, LAI pixels were compared with corresponding eddy covariance GPP data from the 13 sites in the ICOS–Warm Winter 2020 dataset. GPP estimates based on the nighttime partitioning method of net ecosystem exchange (NEE) with variable friction velocity (USTAR) threshold filtering were used and aggregated to the same temporal resolution as the LAI data by calculating 10-day mean values. GEOV2 LAI data showed a strong correlation (r = 0.83) with ICOS GPP data across both time and space (fig. S7B).

All standardized anomaly indexes were calculated on the basis of one equation. For instance, SALAI was calculated on the basis of Eq. 2 (*116*)

$$\mathrm{SALAI}(t) = \frac{\mathrm{LAI}(t) - \overline{\mathrm{LAI}(t)}}{\sigma(t)} \quad (2)$$

where $\mathrm{SALAI}(t)$ is the SALAI at time t, $\mathrm{LAI}(t)$ is the LAI value at time t, $\overline{\mathrm{LAI}}$ is the temporal mean of LAI at time t over 14 years, and σ is the SD of LAI. All standardized anomaly indexes were interpolated to daily time scale.

The ecosystem types within which the drought and the vegetation responses occurred were classified on the basis of the Copernicus Climate Change Service (C3S) 2018 land cover (LC) map (*125*). This dataset uses a consistent classification as the Land Cover Climate Change Initiative (CCI) from the European Space Agency (ESA). These land cover data were available at 300 m resolution across Europe (https://maps.elie.ucl.ac.be/CCI/viewer/).

All data were reprojected to WGS84 and processed on a common grid with 0.01° resolution. Drought and drought impacts were considered only for the vegetation life cycle. Therefore, drought index SPEI and all standardized anomaly indexes (SAET, SANDII, and SALAI) were extracted within the vegetation phenology defined by the start (SOS) and end of season (EOS) in each pixel. The SOS and EOS of vegetation were calculated by the software TIMESAT (*126*, *127*) on the basis of LAI data, and they are consistent with SOS and EOS from Modis phenology products (*117*).

The onset and severity of drought were calculated on the basis of the drought index SPEI. SPEI values lower than −0.5 were recognized as drought. The total number of days with SPEI values lower than −0.5 was defined as drought duration, and the sum of these values was defined as drought severity. Drought with longest duration was identified and its onset date was calculated to capture the main start date. The onset and magnitude (i.e., severity) of the decreases in vegetation physiological attributes (i.e., vegetation anomalies) were calculated on the basis of the same method, with the severity defined as the sum of standardized anomaly values (SAET, SANDII, and SALAI) lower than −1 and the onset as the start of the longest anomaly event.

To reduce the impacts of other disturbances than drought on the analysis, areas with frequent fire (sum of fires in the 24 months greater than the 95th percentile) were eliminated on the basis of the 2017–2018 monthly fire data from NASA Earth Observations. Pixels with a peak LAI value in 2017–2018 less than 0.4 were removed as we consider these pixels as bare ground or areas with very sparse vegetation. Pixels with outliers beyond the 0.02th percentile of the vegetation anomaly magnitudes in ET, NDII, and LAI were also removed. These thresholds were chosen to remove external interferences while keeping as many pixels as possible. Only pixels under drought were considered in the analysis.

To validate the vegetation anomalies results from remote sensing data, vegetation anomalies calculated from remote sensing–based ET and LAI were compared with those from in situ ET and GPP, in which both datasets showed similar magnitudes of anomalies (fig. S8A). Vegetation anomalies calculated from remote sensing–based NDII were compared with anomalies based on LPDR v2 VOD derived from the Advanced Microwave Scanning Radiometer for EOS (AMSR-E) and the Advanced Microwave Scanning Radiometer 2 (AMSR2) (*128*, *129*). Daytime X-band (10.7 GHz) VOD data (overpassing at 1:30 p.m.) were used for the comparison, as these data mainly reflect plant hydraulic regulation. LPDR VOD data are available at a 25-km resolution, which is much coarser than the 1-km resolution of NDII. The magnitudes of anomalies calculated from these two datasets were compared at 25-km resolution, and only pixels with relatively homogeneous LC were selected. Specifically, the main LC types and their proportions were calculated for each pixel, and only pixels with a proportion greater than 75% of a single LC type within the 25-km^2 area were used for the comparison. LPDR X-band VOD data from 2004 to 2018 were used to calculate vegetation anomalies, except for the discontinuous data in 2011–2012 due to the transition from AMSR-E to AMSR2. Based on the comparison, we found that NDII derived from remote sensing is generally capable of capturing vegetation water content dynamics in response to drought in ecosystems (fig. S8B).

Accumulated loss in vegetation physiological attributes

To explore how the regulation of three physiological attributes at ecosystem scale changed with drought in 2018, the accumulated losses in these attributes were obtained by calculating the accumulated anomalies in the three attributes (anomalies in ET, NDII, and LAI) for each pixel. Then, the average response of each individual vegetation attribute over time for each ecosystem was calculated on the basis of all accumulated losses in every pixel for this ecosystem. The average accumulated drought severity over time was calculated on the basis of the same method, which was calculated on the basis of the accumulation of SPEI values lower than −0.5 in each pixel. The average onset and end date of the decrease in the three vegetation attributes were calculated on the basis of the values of the longest anomaly events in each ecosystem type, averaged across all pixels of each ecosystem type.

Paired *t* tests were used to evaluate whether differences in accumulated loss values across pairs of vegetation attributes at specific time points (middle and end of drought) were significant. These accumulated loss values represent the individual measurements that contributed to the average within each ecosystem type.

Ecosystem strategy changes with drought severity

To evaluate the changes in the onset of ecosystem regulation along a range of drought severities, first, the differences between the onset of decrease in vegetation attributes (onset of decrease in ET, NDII, and LAI) and drought onset were calculated at each pixel to represent the relative onset of ecosystem regulation. Then, the average values of these relative onsets (ET relative onset, NDII relative onset, and LAI relative onset) at each drought severity level were calculated in each ecosystem type. Drought severity was divided into six levels (with severities of 0 to ~−600).

Similarly, to investigate changes in the magnitude of ecosystem regulation with drought severity, average magnitude values of ET, NDII, and LAI decrease were calculated for the different drought severity levels. To facilitate the comparison of the decrease magnitude in three vegetation attributes, all values were first scaled to 0-1 by min-max normalization. Minimum and maximum values were determined from the responses across all pixels while taking the 0.1th percentile value as the minimum to avoid abnormal minimum values.

Also, to investigate how ecosystem regulation changes with drought severity in arid and humid regions, average relative onset and magnitude of decrease in ET, NDII, and LAI were calculated at different drought severity levels for humid and arid regions, respectively. Arid and humid regions were classified on the basis of the global aridity index data (*130*), with a threshold of 0.65. In addition, variance partitioning was used to assess the contributions of aridity and drought severity to vegetation anomalies.

Supplementary Materials

This PDF file includes:

Figs. S1 to S8
Tables S1 to S3

REFERENCES AND NOTES

1. D. R. Easterling, G. A. Meehl, C. Parmesan, S. A. Changnon, T. R. Karl, L. O. Mearns, Climate extremes: Observations, modeling, and impacts. *Science* **289**, 2068–2074 (2000).
2. C. B. Field, V. Barros, T. F. Stocker, Q. Dahe, D. Jon Dokken, K. L. Ebi, M. D. Mastrandrea, K. J. Mach, G. K. Plattner, S. K. Allen, M. Tignor, P. M. Midgley, *Managing the Risks of Extreme Events and Disasters to Advance Climate Change Adaptation: Special Report of the Intergovernmental Panel on Climate Change* (Cambridge Univ. Press, 2012).
3. J. I. Christian, E. R. Martin, J. B. Basara, J. C. Furtado, J. A. Otkin, L. E. L. Lowman, E. D. Hunt, V. Mishra, X. Xiao, Global projections of flash drought show increased risk in a warming climate. *Commun. Earth Environ.* **4**, 165 (2023).
4. S. Sun, G. Sun, P. Caldwell, S. McNulty, E. Cohen, J. Xiao, Y. Zhang, Drought impacts on ecosystem functions of the U.S. National Forests and Grasslands: Part II assessment results and management implications. *For. Ecol. Manage.* **353**, 269–279 (2015).
5. S. M. Vicente-Serrano, S. M. Quiring, M. Peña-Gallardo, S. Yuan, F. Domínguez-Castro, A review of environmental droughts: Increased risk under global warming? *Earth Sci. Rev.* **201**, 102953 (2020).
6. C. Werner, L. K. Meredith, S. N. Ladd, J. Ingrisch, A. Kübert, J. van Haren, M. Bahn, K. Bailey, I. Bamberger, M. Beyer, D. Blomdahl, J. Byron, E. Daber, J. Deleeuw, M. A. Dippold, J. Fudyma, J. Gil-Loaiza, L. K. Honeker, J. Hu, J. Huang, T. Klüpfel, J. Krechmer, J. Kreuzwieser, K. Kühnhammer, M. M. Lehmann, K. Meeran, P. K. Misztal, W. R. Ng, E. Pfannerstill, G. Pugliese, G. Purser, J. Roscioli, L. Shi, M. Tfaily, J. Williams, Ecosystem fluxes during drought and recovery in an experimental forest. *Science* **374**, 1514–1518 (2021).
7. W. R. L. Anderegg, A. G. Konings, A. T. Trugman, K. Yu, D. R. Bowling, R. Gabbitas, D. S. Karp, S. Pacala, J. S. Sperry, B. N. Sulman, N. Zenes, Hydraulic diversity of forests regulates ecosystem resilience during drought. *Nature* **561**, 538–541 (2018).
8. M. K. Van der Molen, A. J. Dolman, P. Ciais, T. Eglin, N. Gobron, B. E. Law, P. Meir, W. Peters, O. L. Phillips, M. Reichstein, T. Chen, S. C. Dekker, M. Doubková, M. A. Friedl, M. Jung, B. J. J. M. van den Hurk, R. A. M. de Jeu, B. Kruijt, T. Ohta, K. T. Rebel, S. Plummer, S. I. Seneviratne, S. Sitch, A. J. Teuling, G. R. van der Werf, G. Wang, Drought and ecosystem carbon cycling. *Agric. For. Meteorol.* **151**, 765–773 (2011).
9. F. Volaire, A unified framework of plant adaptive strategies to drought: Crossing scales and disciplines. *Glob. Chang. Biol.* **24**, 2929–2938 (2018).
10. P. J. Mitchell, A. P. O'Grady, D. T. Tissue, D. A. White, M. L. Ottenschlaeger, E. A. Pinkard, Drought response strategies define the relative contributions of hydraulic dysfunction and carbohydrate depletion during tree mortality. *New Phytol.* **197**, 862–872 (2013).
11. R. P. Skelton, A. G. West, T. E. Dawson, Predicting plant vulnerability to drought in biodiverse regions using functional traits. *Proc. Natl. Acad. Sci. U.S.A.* **112**, 5744–5749 (2015).
12. A. L. Pivovaroff, S. C. Pasquini, M. E. De Guzman, K. P. Alstad, J. S. Stemke, L. S. Santiago, Multiple strategies for drought survival among woody plant species. *Funct. Ecol.* **30**, 517–526 (2016).
13. M. Férriz, D. Martin-Benito, I. Cañellas, G. Gea-Izquierdo, Sensitivity to water stress drives differential decline and mortality dynamics of three co-occurring conifers with different drought tolerance. *For. Ecol. Manage.* **486**, 118964 (2021).
14. K. Rao, W. R. L. Anderegg, A. Sala, J. Martínez-Vilalta, A. G. Konings, Satellite-based vegetation optical depth as an indicator of drought-driven tree mortality. *Remote Sens. Environ.* **227**, 125–136 (2019).
15. W. R. L. Anderegg, T. Klein, M. Bartlett, L. Sack, A. F. A. Pellegrini, B. Choat, S. Jansen, Meta-analysis reveals that hydraulic traits explain cross-species patterns of drought-induced tree mortality across the globe. *Proc. Natl. Acad. Sci. U.S.A.* **113**, 5024–5029 (2016).
16. N. McDowell, W. T. Pockman, C. D. Allen, D. D. Breshears, N. Cobb, T. Kolb, J. Plaut, J. Sperry, A. West, D. G. Williams, E. A. Yepez, Mechanisms of plant survival and mortality during drought: Why do some plants survive while others succumb to drought? *New Phytol.* **178**, 719–739 (2008).
17. N. G. McDowell, D. J. Beerling, D. D. Breshears, R. A. Fisher, K. F. Raffa, M. Stitt, The interdependence of mechanisms underlying climate-driven vegetation mortality. *Trends Ecol. Evol.* **26**, 523–532 (2011).
18. F. Tardieu, T. Simonneau, Variability among species of stomatal control under fluctuating soil water status and evaporative demand: Modelling isohydric and anisohydric behaviours. *J. Exp. Bot.* **49**, 419–432 (1998).
19. T. Klein, The variability of stomatal sensitivity to leaf water potential across tree species indicates a continuum between isohydric and anisohydric behaviours. *Funct. Ecol.* **28**, 1313–1320 (2014).
20. J. Martínez-Vilalta, R. Poyatos, D. Aguadé, J. Retana, M. Mencuccini, A new look at water transport regulation in plants. *New Phytol.* **204**, 105–115 (2014).
21. H. G. Jones, Stomatal control of photosynthesis and transpiration. *J. Exp. Bot.* **49**, 387–398 (1998).
22. N. Martin-StPaul, S. Delzon, H. Cochard, Plant resistance to drought depends on timely stomatal closure. *Ecol. Lett.* **20**, 1437–1447 (2017).
23. R. M. Marchin, D. Backes, A. Ossola, M. R. Leishman, M. G. Tjoelker, D. S. Ellsworth, Extreme heat increases stomatal conductance and drought-induced mortality risk in vulnerable plant species. *Glob. Chang. Biol.* **28**, 1133–1146 (2022).
24. J. Martínez-Vilalta, N. Garcia-Forner, Water potential regulation, stomatal behaviour and hydraulic transport under drought: Deconstructing the iso/anisohydric concept. *Plant Cell Environ.* **40**, 962–976 (2017).
25. C. Leuschner, F. Schipka, K. Backes, Stomatal regulation and water potential variation in European beech: Challenging the iso/anisohydry concept. *Tree Physiol.* **42**, 365–378 (2022).
26. I. R. Cowan, "Regulation of water use in relation to carbon gain in higher plants," in *Physiological Plant Ecology II*, B. O. L. Lange, P. S. Nobel, C. B. Osmond, H. Ziegler, Eds. (Springer, 1982), pp. 589–613.
27. B. T. Wolfe, J. S. Sperry, T. A. Kursar, Does leaf shedding protect stems from cavitation during seasonal droughts? A test of the hydraulic fuse hypothesis. *New Phytol.* **212**, 1007–1018 (2016).
28. S. Munné-Bosch, L. Alegre, Die and let live: Leaf senescence contributes to plant survival under drought stress. *Funct. Plant Biol.* **31**, 203–216 (2004).
29. W. M. Jolly, S. W. Running, Effects of precipitation and soil water potential on drought deciduous phenology in the Kalahari. *Glob. Chang. Biol.* **10**, 303–308 (2004).
30. W. H. Schlesinger, M. C. Dietze, R. B. Jackson, R. P. Phillips, C. C. Rhoades, L. E. Rustad, J. M. Vose, Forest biogeochemistry in response to drought. *Glob. Chang. Biol.* **22**, 2318–2328 (2016).
31. N. G. Mcdowell, R. A. Fisher, C. Xu, J. C. Domec, T. Hölttä, D. S. Mackay, J. S. Sperry, A. Boutz, L. Dickman, N. Gehres, J. M. Limousin, A. Macalady, J. Martínez-Vilalta, M. Mencuccini, J. A. Plaut, J. Ogée, R. E. Pangle, D. P. Rasse, M. G. Ryan, S. Sevanto, R. H. Waring, A. P. Williams, E. A. Yepez, W. T. Pockman, Evaluating theories of drought-induced vegetation mortality using a multimodel–experiment framework. *New Phytol.* **200**, 304–321 (2013).
32. M. K. Bartletta, T. Klein, S. Jansen, B. Choat, L. Sack, The correlations and sequence of plant stomatal, hydraulic, and wilting responses to drought. *Proc. Natl. Acad. Sci. U.S.A.* **113**, 13098–13103 (2016).
33. A. T. Trugman, L. D. L. Anderegg, J. D. Shaw, W. R. L. Anderegg, Trait velocities reveal that mortality has driven widespread coordinated shifts in forest hydraulic trait composition. *Proc. Natl. Acad. Sci. U.S.A.* **117**, 8532–8538 (2020).
34. U. Hochberg, F. E. Rockwell, N. M. Holbrook, H. Cochard, Iso/anisohydry: A plant–environment interaction rather than a simple hydraulic trait. *Trends Plant Sci.* **23**, 112–120 (2018).
35. W. A. Hoffmann, R. M. Marchin, P. Abit, O. L. Lau, Hydraulic failure and tree dieback are associated with high wood density in a temperate forest under extreme drought. *Glob. Chang. Biol.* **17**, 2731–2742 (2011).
36. A. AghaKouchak, A. Farahmand, F. S. Melton, J. Teixeira, M. C. Anderson, B. D. Wardlow, C. R. Hain, Remote sensing of drought: Progress, challenges and opportunities. *Rev. Geophys.* **53**, 452–480 (2015).
37. A. G. Konings, P. Gentine, Global variations in ecosystem-scale isohydricity. *Glob. Chang. Biol.* **23**, 891–905 (2017).
38. Y. Zhang, S. Zhou, P. Gentine, X. Xiao, Can vegetation optical depth reflect changes in leaf water potential during soil moisture dry-down events? *Remote Sens. Environ.* **234**, 111451 (2019).
39. M. C. Anderson, C. Hain, B. Wardlow, A. Pimstein, J. R. Mecikalski, W. P. Kustas, Evaluation of drought indices based on thermal remote sensing of evapotranspiration over the continental United States. *J. Climate* **24**, 2025–2044 (2011).
40. W. H. Maes, K. Steppe, Estimating evapotranspiration and drought stress with ground-based thermal remote sensing in agriculture: A review. *J. Exp. Bot.* **63**, 4671–4712 (2012).
41. M. C. Anderson, C. A. Zolin, C. R. Hain, K. Semmens, M. Tugrul Yilmaz, F. Gao, Comparison of satellite-derived LAI and precipitation anomalies over Brazil with a thermal infrared-based evaporative stress index for 2003-2013. *J. Hydrol.* **526**, 287–302 (2015).
42. R. Doughty, P. Köhler, C. Frankenberg, T. S. Magney, X. Xiao, Y. Qin, X. Wu, B. Moore, TROPOMI reveals dry-season increase of solar-induced chlorophyll fluorescence in the Amazon forest. *Proc. Natl. Acad. Sci. U.S.A.* **116**, 22393–22398 (2019).
43. M. Zhang, X. Yuan, Z. Zeng, M. Pan, P. Wu, J. Xiao, T. F. Keenan, A pronounced decline in northern vegetation resistance to flash droughts from 2001 to 2022. *Nat. Commun.* **16**, 2984 (2025).
44. W. Yuan, Y. Zheng, S. Piao, P. Ciais, D. Lombardozzi, Y. Wang, Y. Ryu, G. Chen, W. Dong, Z. Hu, A. K. Jain, C. Jiang, E. Kato, S. Li, S. Lienert, S. Liu, J. E. M. S. Nabel, Z. Qin, T. Quine,

S. Sitch, W. K. Smith, F. Wang, C. Wu, Z. Xiao, S. Yang, Increased atmospheric vapor pressure deficit reduces global vegetation growth. *Sci. Adv.* **5**, eaax1396 (2019).
45. W. Li, J. Pacheco-Labrador, M. Migliavacca, D. Miralles, A. Hoek van Dijke, M. Reichstein, M. Forkel, W. Zhang, C. Frankenberg, A. Panwar, Q. Zhang, U. Weber, P. Gentine, R. Orth, Widespread and complex drought effects on vegetation physiology inferred from space. *Nat. Commun.* **14**, 4640 (2023).
46. P. F. Scholander, H. T. Hammel, E. D. Bradstreet, E. A. Hemmingsen, Sap pressure in vascular plants. *Science* **148**, 339–346 (1965).
47. M. T. Tyree, H. T. Hammel, The measurement of the turgor pressure and the water relations of plants by the pressure-bomb technique. *J. Exp. Bot.* **23**, 267–282 (1972).
48. H. Richter, A diagram for the description of water relations in plant cells and organs. *J. Exp. Bot.* **29**, 1197–1203 (1978).
49. A. G. Konings, S. S. Saatchi, C. Frankenberg, M. Keller, V. Leshyk, W. R. L. Anderegg, V. Humphrey, A. M. Matheny, A. Trugman, L. Sack, E. Agee, M. L. Barnes, O. Binks, K. Cawse-Nicholson, B. O. Christoffersen, D. Entekhabi, P. Gentine, N. M. Holtzman, G. G. Katul, Y. Liu, M. Longo, J. Martinez-Vilalta, N. McDowell, P. Meir, M. Mencuccini, A. Mrad, K. A. Novick, R. S. Oliveira, P. Siqueira, S. C. Steele-Dunne, D. R. Thompson, Y. Wang, R. Wehr, J. D. Wood, X. Xu, P. A. Zuidema, Detecting forest response to droughts with global observations of vegetation water content. *Glob. Chang. Biol.* **27**, 6005–6024 (2021).
50. D. Nadal-Sala, R. Grote, B. Birami, T. Knüver, R. Rehschuh, S. Schwarz, N. K. Ruehr, Leaf shedding and non-stomatal limitations of photosynthesis mitigate hydraulic conductance losses in scots pine saplings during severe drought stress. *Front. Plant Sci.* **12**, 1600 (2021).
51. D. D. Baldocchi, S. Ma, S. Rambal, L. Misson, J. M. Ourcival, J. M. Limousin, J. Pereira, D. Papale, On the differential advantages of evergreenness and deciduousness in mediterranean oak woodlands: A flux perspective. *Ecol. Appl.* **20**, 1583–1597 (2010).
52. S. J. Bucci, F. G. Scholz, P. I. Campanello, L. Montti, M. Jimenez-Castillo, F. A. Rockwell, L. La Manna, P. Guerra, P. L. Bernal, O. Troncoso, J. Enricci, M. N. Holbrook, G. Goldstein, Hydraulic differences along the water transport system of South American Nothofagus species: Do leaves protect the stem functionality? *Tree Physiol.* **32**, 880–893 (2012).
53. M. T. Tyree, J. S. Sperry, Vulnerability of xylem to cavitation and embolism. *Annu. Rev. Plant. Physiol. Plant. Mol. Biol.* **40**, 19–36 (1989).
54. M. Arend, R. M. Link, R. Patthey, G. Hoch, B. Schuldt, A. Kahmen, Rapid hydraulic collapse as cause of drought-induced mortality in conifers. *Proc. Natl. Acad. Sci. U.S.A.* **118**, e2025251118 (2021).
55. P. B. Reich, M. B. Walters, D. S. Ellsworth, From tropics to tundra: Global convergence in plant functioning. *Proc. Natl. Acad. Sci. U.S.A.* **94**, 13730–13734 (1997).
56. R. L. Salomón, R. L. Peters, R. Zweifel, U. G. W. Sass-Klaassen, A. I. Stegehuis, M. Smiljanic, R. Poyatos, F. Babst, E. Cienciala, P. Fonti, B. J. W. Lerink, M. Lindner, J. Martinez-Vilalta, M. Mencuccini, G. J. Nabuurs, E. van der Maaten, G. von Arx, A. Bär, L. Akhmetzyanov, D. Balanzategui, M. Bellan, J. Bendix, D. Berveiller, M. Blaženec, V. Čada, V. Carraro, S. Cecchini, T. Chan, M. Conedera, N. Delpierre, S. Delzon, Ľ. Ditmarová, J. Dolezal, E. Dufrêne, J. Edvardsson, S. Ehekircher, A. Forner, J. Frouz, A. Ganthaler, V. Gryc, A. Güney, I. Heinrich, R. Hentschel, P. Janda, M. Ježík, H. P. Kahle, S. Knüsel, J. Krejza, Ł. Kuberski, J. Kučera, F. Lebourgeois, M. Mikoláš, R. Matula, S. Mayr, W. Oberhuber, N. Obojes, B. Osborne, T. Paljakka, R. Plichta, I. Rabbel, C. B. K. Rathgeber, Y. Salmon, M. Saunders, T. Scharnweber, Z. Sitková, D. F. Stangler, K. Stereńczak, M. Stojanović, K. Střelcová, J. Světlík, M. Svoboda, B. Tobin, V. Trotsiuk, J. Urban, F. Valladares, H. Vavrčík, M. Vejpustková, L. Walthert, M. Wilmking, E. Zin, J. Zou, K. Steppe, The 2018 European heatwave led to stem dehydration but not to consistent growth reductions in forests. *Nat. Commun.* **13**, 28 (2022).
57. R. Villar, J. Merino, Comparison of leaf construction costs in woody species with differing leaf life-spans in contrasting ecosystems. *New Phytol.* **151**, 213–226 (2001).
58. J. Carnicer, A. Barbeta, D. Sperlich, M. Coll, J. Penuelas, Contrasting trait syndromes in angiosperms and conifers are associated with different responses of tree growth to temperature on a large scale. *Front. Plant Sci.* **4**, 409 (2013).
59. C. Grossiord, Having the right neighbors: How tree species diversity modulates drought impacts on forests. *New Phytol.* **228**, 42–49 (2020).
60. M. Pardos, M. del Río, H. Pretzsch, H. Jactel, K. Bielak, F. Bravo, G. Brazaitis, E. Defossez, M. Engel, K. Godvod, K. Jacobs, L. Jansone, A. Jansons, X. Morin, A. Nothdurft, L. Oreti, Q. Ponette, M. Pach, J. Riofrío, R. Ruíz-Peinado, A. Tomao, E. Uhl, R. Calama, The greater resilience of mixed forests to drought mainly depends on their composition: Analysis along a climate gradient across Europe. *For. Ecol. Manage.* **481**, 118687 (2021).
61. M. De Cáceres, M. Mencuccini, N. Martin-StPaul, J. M. Limousin, L. Coll, R. Poyatos, A. Cabon, V. Granda, A. Forner, F. Valladares, J. Martínez-Vilalta, Unravelling the effect of species mixing on water use and drought stress in Mediterranean forests: A modelling approach. *Agric. For. Meteorol.* **296**, 108233 (2021).
62. J. Cao, H. Liu, B. Zhao, R. Peng, B. Liang, O. A. Anenkhonov, A. Y. Korolyuk, D. V. Sandanov, Mixed forest suffered less drought stress than pure forest in southern Siberia. *Agric. For. Meteorol.* **325**, 109137 (2022).
63. J. Schwaab, E. L. Davin, P. Bebi, A. Duguay-Tetzlaff, L. T. Waser, M. Haeni, R. Meier, Increasing the broad-leaved tree fraction in European forests mitigates hot temperature extremes. *Sci. Rep.* **10**, 14153 (2020).
64. J. H. Richards, M. M. Caldwell, Hydraulic lift: Substantial nocturnal water transport between soil layers by Artemisia tridentata roots. *Oecologia* **73**, 486–489 (1987).
65. I. Prieto, C. Armas, F. I. Pugnaire, Water release through plant roots: New insights into its consequences at the plant and ecosystem level. *New Phytol.* **193**, 830–841 (2012).
66. A. Fichtner, F. Schnabel, H. Bruelheide, M. Kunz, K. Mausolf, A. Schuldt, W. Härdtle, G. von Oheimb, Neighbourhood diversity mitigates drought impacts on tree growth. *J. Ecol.* **108**, 865–875 (2020).
67. M. Migliavacca, T. Musavi, M. D. Mahecha, J. A. Nelson, J. Knauer, D. D. Baldocchi, O. Perez-Priego, R. Christiansen, J. Peters, K. Anderson, M. Bahn, T. A. Black, P. D. Blanken, D. Bonal, N. Buchmann, S. Caldararu, A. Carrara, N. Carvalhais, A. Cescatti, J. Chen, J. Cleverly, E. Cremonese, A. R. Desai, T. S. El-Madany, M. M. Farella, M. Fernández-Martínez, G. Filippa, M. Forkel, M. Galvagno, U. Gomarasca, C. M. Gough, M. Göckede, A. Ibrom, H. Ikawa, I. A. Janssens, M. Jung, J. Kattge, T. F. Keenan, A. Knohl, H. Kobayashi, G. Kraemer, B. E. Law, M. J. Liddell, X. Ma, I. Mammarella, D. Martini, C. Macfarlane, G. Matteucci, L. Montagnani, D. E. Pabon-Moreno, C. Panigada, D. Papale, E. Pendall, J. Penuelas, R. P. Phillips, P. B. Reich, M. Rossini, E. Rotenberg, R. L. Scott, C. Stahl, U. Weber, G. Wohlfahrt, S. Wolf, I. J. Wright, D. Yakir, S. Zaehle, M. Reichstein, The three major axes of terrestrial ecosystem function. *Nature* **598**, 468–472 (2021).
68. M. G. De Kauwe, B. E. Medlyn, J. Knauer, C. A. Williams, Ideas and perspectives: How coupled is the vegetation to the boundary layer? *Biogeosciences* **14**, 4435–4453 (2017).
69. M. G. Ryan, N. Phillips, B. J. Bond, The hydraulic limitation hypothesis revisited. *Plant Cell Environ.* **29**, 367–381 (2006).
70. Y. S. Lin, B. E. Medlyn, R. A. Duursma, I. C. Prentice, H. Wang, S. Baig, D. Eamus, V. R. De Dios, P. Mitchell, D. S. Ellsworth, M. O. De Beeck, G. Wallin, J. Uddling, L. Tarvainen, M. L. Linderson, L. A. Cernusak, J. B. Nippert, T. W. Ocheltree, D. T. Tissue, N. K. Martin-StPaul, A. Rogers, J. M. Warren, P. De Angelis, K. Hikosaka, Q. Han, Y. Onoda, T. E. Gimeno, C. V. M. Barton, J. Bennie, D. Bonal, A. Bosc, M. Löw, C. Macinins-Ng, A. Rey, L. Rowland, S. A. Setterfield, S. Tausz-Posch, J. Zaragoza-Castells, M. S. J. Broadmeadow, J. E. Drake, M. Freeman, O. Ghannoum, L. B. Hutley, J. W. Kelly, K. Kikuzawa, P. Kolari, K. Koyama, J. M. Limousin, P. Meir, A. C. L. Da Costa, T. N. Mikkelsen, N. Salinas, W. Sun, L. Wingate, Optimal stomatal behaviour around the world. *Nat. Clim. Chang.* **5**, 459–464 (2015).
71. N. Nicolai-Shaw, J. Zscheischler, M. Hirschi, L. Gudmundsson, S. I. Seneviratne, A drought event composite analysis using satellite remote-sensing based soil moisture. *Remote Sens. Environ.* **203**, 216–225 (2017).
72. H.-j. Xu, X.-p. Wang, C.-y. Zhao, X.-m. Yang, Diverse responses of vegetation growth to meteorological drought across climate zones and land biomes in northern China from 1981 to 2014. *Agric. For. Meteorol.* **262**, 1–13 (2018).
73. P. Parolin, C. Lucas, M. T. F. Piedade, F. Wittmann, Drought responses of flood-tolerant trees in Amazonian floodplains. *Ann. Bot.* **105**, 129–139 (2010).
74. E. Naumburg, R. Mata-Gonzalez, R. G. Hunter, T. McLendon, D. W. Martin, Phreatophytic vegetation and groundwater fluctuations: A review of current research and application of ecosystem response modeling with an emphasis on great basin vegetation. *Environ. Manag.* **35**, 726–740 (2005).
75. P. Parolin, Flood-tolerant trees of Amazonian floodplains. *Pesqui. Bot.* **61**, 7–38 (2010).
76. B. W. Touchette, A. Frank, L. R. Iannacone, G. Turner, Drought susceptibility in emergent wetland angiosperms: A comparison of water deficit growth in five herbaceous perennials. *Wetl. Ecol. Manag.* **16**, 485–497 (2008).
77. N. Saintilan, K. Rogers, Woody plant encroachment of grasslands: A comparison of terrestrial and wetland settings. *New Phytol.* **205**, 1062–1070 (2015).
78. N. Saintilan, S. Bowen, O. Maguire, S. S. Karimi, L. Wen, M. Powell, M. J. Colloff, S. Sandi, P. Saco, J. Rodriguez, Resilience of trees and the vulnerability of grasslands to climate change in temperate Australian wetlands. *Landsc. Ecol.* **36**, 803–814 (2021).
79. M. K. Bartlett, C. Scoffoni, L. Sack, The determinants of leaf turgor loss point and prediction of drought tolerance of species and biomes: A global meta-analysis. *Ecol. Lett.* **15**, 393–405 (2012).
80. J. Canadell, R. B. Jackson, J. R. Ehleringer, H. A. Mooney, O. E. Sala, E. D. Schulze, Maximum rooting depth of vegetation types at the global scale. *Oecologia* **108**, 583–595 (1996).
81. A. Kulmatiski, K. H. Beard, Root niche partitioning among grasses, saplings, and trees measured using a tracer technique. *Oecologia* **171**, 25–37 (2013).
82. A. Farjon, *A Handbook of the World's Conifers* (Brill, 2010), vol. 1.
83. F. Da Ronch, G. Caudullo, W. Tinner, D. de Rigo, "Larix decidua and other larches in Europe: Distribution, habitat, usage and threats," in *European Atlas of Forest Tree Species*, J. San-Miguel-Ayanz, D. de Rigo, G. Caudullo, T. Houston Durrant, A. Mauri, Eds. (Publication Office of the European Union, 2016), p. 108.
84. A. Badalotti, T. Anfodillo, J. Grace, Evidence of osmoregulation in *Larix decidua* at Alpine treeline and comparative responses to water availability of two co-occurring evergreen species. *Ann. For. Sci.* **57**, 623–633 (2000).

85. M. Leo, W. Oberhuber, R. Schuster, T. E. E. Grams, R. Matyssek, G. Wieser, Evaluating the effect of plant water availability on inner alpine coniferous trees based on sap flow measurements. *Eur. J. For. Res.* **133**, 691–698 (2014).
86. G. Wieser, W. Oberhuber, A. Gruber, F. Oberleitner, R. Hasibeder, M. Bahn, Artificial top soil drought hardly affects water use of *Picea abies* and *Larix decidua* saplings at the treeline in the Austrian alps. *Forests* **10**, 777 (2019).
87. B. Eilmann, A. Rigling, Tree-growth analyses to estimate tree species' drought tolerance. *Tree Physiol.* **32**, 178–187 (2012).
88. M. Lévesque, A. Rigling, H. Bugmann, P. Weber, P. Brang, Growth response of five co-occurring conifers to drought across a wide climatic gradient in Central Europe. *Agric. For. Meteorol.* **197**, 1–12 (2014).
89. J. Charlet de Sauvage, H. Bugmann, C. Bigler, M. Lévesque, Species diversity and competition have minor effects on the growth response of silver fir, European larch and Douglas fir to drought. *Agric. For. Meteorol.* **341**, 109664 (2023).
90. R. Valentini, T. Anfodillo, J. R. Ehleringer, Water sources and carbon isotope composition ($\delta^{13}C$) of selected tree species of the Italian Alps. *Can. J. For. Res.* **24**, 1575–1578 (1994).
91. T. Anfodillo, S. Rento, V. Carraro, L. Furlanetto, C. Urbinati, M. Carrer, Tree water relations and climatic variations at the alpine timberline: Seasonal changes of sap flux and xylem water potential in Larix decidua Miller, Picea abies (L.) Karst. and *Pinus cembra* L. *Ann. For. Sci.* **55**, 159–172 (1998).
92. N. Obojes, A. Meurer, C. Newesely, E. Tasser, W. Oberhuber, S. Mayr, U. Tappeiner, Water stress limits transpiration and growth of European larch up to the lower subalpine belt in an inner-alpine dry valley. *New Phytol.* **220**, 460–475 (2018).
93. W. R. L. Anderegg, Spatial and temporal variation in plant hydraulic traits and their relevance for climate change impacts on vegetation. *New Phytol.* **205**, 1008–1014 (2015).
94. P. Papastefanou, C. S. Zang, T. A. M. Pugh, D. Liu, T. E. E. Grams, T. Hickler, A. Rammig, A dynamic model for strategies and dynamics of plant water-potential regulation under drought conditions. *Front. Plant Sci.* **11**, 516681 (2020).
95. K. E. Trenberth, A. Dai, G. Van Der Schrier, P. D. Jones, J. Barichivich, K. R. Briffa, J. Sheffield, Global warming and changes in drought. *Nat. Clim. Chang.* **4**, 17–22 (2014).
96. C. D. Allen, A. K. Macalady, H. Chenchouni, D. Bachelet, N. McDowell, M. Vennetier, T. Kitzberger, A. Rigling, D. D. Breshears, E. H.(T.) Hogg, P. Gonzalez, R. Fensham, Z. Zhang, J. Castro, N. Demidova, J.-H. Lim, G. Allard, S. W. Running, A. Semerci, N. Cobb, A global overview of drought and heat-induced tree mortality reveals emerging climate change risks for forests. *For. Ecol. Manage.* **259**, 660–684 (2010).
97. C. Senf, A. Buras, C. S. Zang, A. Rammig, R. Seidl, Excess forest mortality is consistently linked to drought across Europe. *Nat. Commun.* **11**, 6200 (2020).
98. E. Batllori, F. Lloret, T. Aakala, W. R. L. Anderegg, E. Aynekulu, D. P. Bendixsen, A. Bentouati, C. Bigler, C. J. Burk, J. J. Camarero, M. Colangelo, J. D. Coop, R. Fensham, M. L. Floyd, L. Galiano, J. L. Ganey, P. Gonzalez, A. L. Jacobsen, J. M. Kane, T. Kitzberger, J. C. Linares, S. B. Marchetti, G. Matusick, M. Michaelia, R. M. Navarro-Cerrillo, R. B. Pratt, M. D. Redmond, A. Rigling, F. Ripullone, G. Sangüesa-Barreda, Y. Sasal, S. Saura-Mas, M. L. Suarez, T. T. Veblen, A. Vilà-Cabrera, C. Vincke, B. Zeeman, Forest and woodland replacement patterns following drought-related mortality. *Proc. Natl. Acad. Sci. U.S.A.* **117**, 29720–29729 (2020).
99. W. R. L. Anderegg, J. M. Kane, L. D. L. Anderegg, Consequences of widespread tree mortality triggered by drought and temperature stress. *Nat. Clim. Chang.* **3**, 30–36 (2013).
100. A. Kilic, R. G., J. Kjaersgaard, J. Huntington, B. Kamble, R. Trezza, I. Ratcliffe, "Operational remote sensing of ET and challenges," in *Evapotranspiration - Remote Sensing and Modeling* (InTech, 2012), pp. 467–492.
101. J. L. Monteith, Evaporation and environment. *Symp. Soc. Exp. Biol.* **19**, 205–234 (1965).
102. K. Wang, R. E. Dickinson, A review of global terrestrial evapotranspiration: Observation, modeling, climatology, and climatic variability. *Rev. Geophys.* **50**, 2005 (2012).
103. G. B. Senay, S. Kagone, N. M. Velpuri, Operational global actual evapotranspiration: Development, evaluation, and dissemination. *Sensors* **20**, 1915 (2020).
104. C. J. Tucker, Remote sensing of leaf water content in the near infrared. *Remote Sens. Environ.* **10**, 23–32 (1980).
105. M. A. Hardisky, V. Klemas, R. M. Smart, The influence of soil salinity, growth form, and leaf moisture on the spectral radiance of Spartina alterniflora canopies. *Photogramm. Eng. Remote Sens.* **49**, 77–83 (1983).
106. M. T. Yilmaz, E. R. Hunt, T. J. Jackson, Remote sensing of vegetation water content from equivalent water thickness using satellite imagery. *Remote Sens. Environ.* **112**, 2514–2522 (2008).
107. X. Zhu, Q. Li, C. Guo, Evaluation of the monitoring capability of various vegetation indices and mainstream satellite band settings for grassland drought. *Ecol. Inform.* **82**, 102717 (2024).
108. F. Liu, H. Liu, C. Xu, L. Shi, X. Zhu, Y. Qi, W. He, Old-growth forests show low canopy resilience to droughts at the southern edge of the taiga. *Glob. Chang. Biol.* **27**, 2392–2402 (2021).
109. P. Ceccato, S. Flasse, J. M. Grégoire, Designing a spectral index to estimate vegetation water content from remote sensing data: Part 1: Theoretical approach. *Remote Sens. Environ.* **82**, 188–197 (2002).
110. L. Serrano, S. L. Ustin, D. A. Roberts, J. A. Gamon, J. Peñuelas, Deriving water content of chaparral vegetation from AVIRIS data. *Remote Sens. Environ.* **74**, 570–581 (2000).
111. A. R. Huete, A soil-adjusted vegetation index (SAVI). *Remote Sens. Environ.* **25**, 295–309 (1988).
112. D. B. Lobell, G. P. Asner, Moisture effects on soil reflectance. *Soil Sci. Soc. Am. J.* **66**, 722–727 (2002).
113. A. F. Van Loon, Hydrological drought explained. *Wiley Interdiscip. Rev. Water* **2**, 359–392 (2015).
114. A. Toreti, Gridded agro-meteorological data in Europe, European Commission, Joint Research Centre (JRC) (2014); http://data.europa.eu/89h/jrc-marsop4-7-weather_obs_grid_2019.
115. S. Running, Q. Mu, M. Zhao, MOD16A2 MODIS/Terra Net evapotranspiration 8-day L4 global 500m SIN grid V006, NASA Land Processes Distributed Active Archive Center (2017); https://doi.org/10.5067/MODIS/MOD16A2.006.
116. Q. Chen, J. Timmermans, W. Wen, P. M. van Bodegom, A multi-metric assessment of drought vulnerability across different vegetation types using high resolution remote sensing. *Sci. Total Environ.* **832**, 154970 (2022).
117. Q. Chen, J. Timmermans, W. Wen, P. M. van Bodegom, Ecosystems threatened by intensified drought with divergent vulnerability. *Remote Sens. Environ.* **289**, 113512 (2023).
118. A. Savitzky, M. J. E. Golay, Smoothing and Differentiation of Data by Simplified Least Squares Procedures. *Anal. Chem.* **36**, 1627–1639 (1964).
119. Warm Winter 2020 Team and ICOS Ecosystem Thematic Centre, Warm Winter 2020 ecosystem eddy covariance flux product for 73 stations in FLUXNET-Archive format—release 2022-1, version 1.0, ICOS Carbon Portal (2022); https://doi.org/10.18160/2G60-ZHAK.
120. M. Reichstein, E. Falge, D. Baldocchi, D. Papale, M. Aubinet, P. Berbigier, C. Bernhofer, N. Buchmann, T. Gilmanov, A. Granier, T. Grünwald, K. Havránková, H. Ilvesniemi, D. Janous, A. Knohl, T. Laurila, A. Lohila, D. Loustau, G. Matteucci, T. Meyers, F. Miglietta, J. M. Ourcival, J. Pumpanen, S. Rambal, E. Rotenberg, M. Sanz, J. Tenhunen, G. Seufert, F. Vaccari, T. Vesala, D. Yakir, R. Valentini, On the separation of net ecosystem exchange into assimilation and ecosystem respiration: Review and improved algorithm. *Glob. Chang. Biol.* **11**, 1424–1439 (2005).
121. G. Pastorello, C. Trotta, E. Canfora, H. Chu, D. Christianson, Y. W. Cheah, C. Poindexter, J. Chen, A. Elbashandy, M. Humphrey, P. Isaac, D. Polidori, A. Ribeca, C. van Ingen, L. Zhang, B. Amiro, C. Ammann, M. A. Arain, J. Ardö, T. Arkebauer, S. K. Arndt, N. Arriga, M. Aubinet, M. Aurela, D. Baldocchi, A. Barr, E. Beamesderfer, L. B. Marchesini, O. Bergeron, J. Beringer, C. Bernhofer, D. Berveiller, D. Billesbach, T. A. Black, P. D. Blanken, G. Bohrer, J. Boike, P. V. Bolstad, D. Bonal, J. M. Bonnefond, D. R. Bowling, R. Bracho, J. Brodeur, C. Brümmer, N. Buchmann, B. Burban, S. P. Burns, P. Buysse, P. Cale, M. Cavagna, P. Cellier, S. Chen, I. Chini, T. R. Christensen, J. Cleverly, A. Collalti, C. Consalvo, B. D. Cook, D. Cook, C. Coursolle, E. Cremonese, P. S. Curtis, E. D'Andrea, H. da Rocha, X. Dai, K. J. Davis, B. De Cinti, A. de Grandcourt, A. De Ligne, R. C. De Oliveira, N. Delpierre, A. R. Desai, C. M. Di Bella, P. di Tommasi, H. Dolman, F. Domingo, G. Dong, S. Dore, P. Duce, E. Dufrêne, A. Dunn, J. Dušek, D. Eamus, U. Eichelmann, H. A. M. ElKhidir, W. Eugster, C. M. Ewenz, B. Ewers, D. Famulari, S. Fares, I. Feigenwinter, A. Feitz, R. Fensholt, G. Filippa, M. Fischer, J. Frank, M. Galvagno, M. Gharun, D. Gianelle, B. Gielen, B. Gioli, A. Gitelson, I. Goded, M. Goeckede, A. H. Goldstein, C. M. Gough, M. L. Goulden, A. Graf, A. Griebel, C. Gruening, T. Grünwald, A. Hammerle, S. Han, X. Han, B. U. Hansen, C. Hanson, J. Hatakka, Y. He, M. Hehn, B. Heinesch, N. Hinko-Najera, L. Hörtnagl, L. Hutley, A. Ibrom, H. Ikawa, M. Jackowicz-Korczynski, D. Janouš, W. Jans, R. Jassal, S. Jiang, T. Kato, M. Khomik, J. Klatt, A. Knohl, S. Knox, H. Kobayashi, G. Koerber, O. Kolle, Y. Kosugi, A. Kotani, A. Kowalski, B. Kruijt, J. Kurbatova, W. L. Kutsch, H. Kwon, S. Launiainen, T. Laurila, B. Law, R. Leuning, Y. Li, M. Liddell, J. M. Limousin, M. Lion, A. J. Liska, A. Lohila, A. López-Ballesteros, E. López-Blanco, B. Loubet, D. Loustau, A. Lucas-Moffat, J. Lüers, S. Ma, C. Macfarlane, V. Magliulo, R. Maier, I. Mammarella, G. Manca, B. Marcolla, H. A. Margolis, S. Marras, W. Massman, M. Mastepanov, R. Matamala, J. H. Matthes, F. Mazzenga, H. McCaughey, I. McHugh, A. M. S. McMillan, L. Merbold, W. Meyer, T. Meyers, S. D. Miller, S. Minerbi, U. Moderow, R. K. Monson, L. Montagnani, C. E. Moore, E. Moors, V. Moreaux, C. Moureaux, J. W. Munger, T. Nakai, J. Neirynck, Z. Nesic, G. Nicolini, A. Noormets, M. Northwood, M. Nosetto, Y. Nouvellon, K. Novick, W. Oechel, J. E. Olesen, J. M. Ourcival, S. A. Papuga, F. J. Parmentier, E. Paul-Limoges, M. Pavelka, M. Peichl, E. Pendall, R. P. Phillips, K. Pilegaard, N. Pirk, G. Posse, T. Powell, H. Prasse, S. M. Prober, S. Rambal, Ü. Rannik, N. Raz-Yaseef, D. Reed, V. R. de Dios, N. Restrepo-Coupe, B. R. Reverter, M. Roland, S. Sabbatini, T. Sachs, S. R. Saleska, E. P. Sánchez-Cañete, Z. M. Sanchez-Mejia, H. P. Schmid, M. Schmidt, K. Schneider, F. Schrader, I. Schroder, R. L. Scott, P. Sedlák, P. Serrano-Ortíz, C. Shao, P. Shi, I. Shironya, L. Siebicke, L. Šigut, R. Silberstein, C. Sirca, D. Spano, R. Steinbrecher, R. M. Stevens, C. Sturtevant, A. Suyker, T. Tagesson, S. Takanashi, Y. Tang, N. Tapper, J. Thom, F. Tiedemann, M. Tomassucci, J. P. Tuovinen, S. Urbanski, R. Valentini, M. van der Molen, E. van Gorsel, K. van Huissteden, A. Varlagin, J. Verfaillie, T. Vesala, C. Vincke, D. Vitale, N. Vygodskaya, J. P. Walker, E. Walter-Shea, H. Wang, R. Weber, S. Westermann, C. Wille, S. Wofsy, G. Wohlfahrt, S. Wolf,

W. Woodgate, Y. Li, R. Zampedri, J. Zhang, G. Zhou, D. Zona, D. Agarwal, S. Biraud, M. Torn, D. Papale, The FLUXNET2015 dataset and the ONEFlux processing pipeline for eddy covariance data. *Sci. Data* **7**, 225 (2021).
122. N. Gorelick, M. Hancher, M. Dixon, S. Ilyushchenko, D. Thau, R. Moore, Google Earth Engine: Planetary-scale geospatial analysis for everyone. *Remote Sens. Environ.* **202**, 18–27 (2017).
123. E. Vermote, MOD09A1 MODIS/terra surface reflectance 8-day L3 global 500m SIN grid V006, NASA Land Processes Distributed Active Archive Center (2015); https://doi.org/10.5067/MODIS/MOD09A1.006.
124. European Union's Copernicus Land Monitoring Service information, Leaf Area Index; https://land.copernicus.eu/en/products/vegetation/leaf-area-index-v2-0-1km, https://doi.org/10.2909/d5fdc595-2e03-4cbe-a39e-5f006f9cef07.
125. Copernicus Climate Change Service, Land cover classification gridded maps from 1992 to present derived from satellite observations, Copernicus Climate Change Service (C3S) Climate Data Store (CDS) (2019); https://doi.org/10.24381/cds.006f2c9a.
126. P. Jönsson, L. Eklundh, Seasonality extraction by function fitting to time-series of satellite sensor data. *IEEE Trans. Geosci. Remote Sens.* **40**, 1824–1832 (2002).
127. P. Jönsson, L. Eklundh, TIMESAT - A program for analyzing time-series of satellite sensor data. *Comput. Geosci.* **30**, 833–845 (2004).
128. J. Du, L. A. Jones, J. S. Kimball, Daily global land surface parameters derived from AMSR-E and AMSR2, version 2 (vegetation optical depth), NASA National Snow and Ice Data Center Distributed Active Archive Center (2017); https://doi.org/10.5067/JIKQZ6WO5C5M.
129. J. Du, J. S. Kimball, L. A. Jones, Y. Kim, J. Glassy, J. D. Watts, A global satellite environmental data record derived from AMSR-E and AMSR2 microwave Earth observations. *Earth Syst. Sci. Data* **9**, 791–808 (2017).
130. R. J. Zomer, J. Xu, A. Trabucco, Version 3 of the Global Aridity Index and Potential Evapotranspiration Database. *Sci. Data* **9**, 409 (2022).

Acknowledgments: We acknowledge the ESA CCI Land Cover and the EC C3S Land Cover project for providing LC map. This publication contains modified Copernicus Climate Change Service information (2021). Neither the European Commission nor ECMWF is responsible for any use that may be made of the Copernicus information or data it contains. This publication has been prepared using European Union's Copernicus Land Monitoring Service information: https://doi.org/10.2909/d5fdc595-2e03-4cbe-a39e-5f006f9cef07. **Funding:** The contribution of Q.C. was funded by the China Scholarship Council (grant no. 201806810030). **Author contributions:** Conceptualization: Q.C., J.T., and P.M.v.B. Methodology: Q.C., J.T., and P.M.v.B. Software: Q.C. and J.T. Validation: Q.C. and P.M.v.B. Formal analysis: Q.C., J.T., and P.M.v.B. Investigation: Q.C. and J.T. Data curation: Q.C. and J.T. Writing—original draft: Q.C. and P.M.v.B. Writing—review and editing: Q.C., J.T., and P.M.v.B. Visualization: Q.C., J.T., and P.M.v.B. Supervision: J.T. and P.M.v.B. Project administration: P.M.v.B. **Competing interests:** The authors declare that they have no competing interests. **Data and materials availability:** All data needed to evaluate the conclusions in the paper are present in the paper and/or the Supplementary Materials. All data originally used in this study are publicly available. JRC MARS precipitation data are available at http://data.europa.eu/89h/jrc-marsop4-7-weather_obs_grid_2019. The MSG-CPP precipitation data are available at https://msgcpp.knmi.nl. MODIS MOD16A2 PET data are available at https://doi.org/10.5067/MODIS/MOD16A2.006. SSEBop ETa data are available at https://earlywarning.usgs.gov/fews/product/461/. Modis MOD09A1 data are available at https://doi.org/10.5067/MODIS/MOD09A1.006. GEOV2 LAI data are available at https://land.copernicus.eu/en/products/vegetation/leaf-area-index-v2-0-1km. NASA Earth Observations fire data are available at https://neo.gsfc.nasa.gov/view.php?datasetId=MOD14A1_M_FIRE. Copernicus Climate Change Service (C3S) 2018 LC map is available at https://maps.elie.ucl.ac.be/CCI/viewer/. ICOS–Warm Winter 2020 data are available at www.icos-cp.eu/data-products/2G60-ZHAK. LPDR v2 VOD data are available at http://files.ntsg.umt.edu/data/LPDR_v2. Global aridity index data are available at https://doi.org/10.6084/m9.figshare.7504448.v5. The main codes used for the analyses are available on Zenodo at https://zenodo.org/records/15643051.

Submitted 25 November 2024
Accepted 27 June 2025
Published 30 July 2025
10.1126/sciadv.adt9251